

Photoisomerization Efficiency of a Solar Thermal Fuel in the Strong Coupling Regime

Jürgen Mony, Clàudia Climent, Anne Ugleholdt Petersen, Kasper Moth-Poulsen, Johannes Feist,* and Karl Börjesson*

Strong exciton-photon coupling is achieved when the interaction between molecules and an electromagnetic field is increased to a level where they cannot be treated as separate systems. This leads to the formation of polaritonic states and an effective rearrangement of the potential energy surfaces, which opens the possibility to modify photochemical reactions. This work investigates how the strong coupling regime is affecting the photoisomerization efficiency and thermal backconversion of a norbornadiene–quadricyclane molecular photoswitch. The quantum yield of photoisomerization shows both an excitation wavelength and exciton/photon constitution dependence. The polariton-induced decay and energy transfer processes are discussed to be the reason for this finding. Furthermore, the thermal back conversion of the system is unperturbed and the lower polariton effectively shifts the absorption onset to lower energies. The reason for the unperturbed thermal backconversion is that it occurs on the ground state, which is unaffected. This work demonstrates how strong coupling can change material properties towards higher efficiencies in applications. Importantly, the experiments illustrate that strong coupling can be used to optimize the absorption onset of the molecular photoswitch norbornadiene without affecting the back reaction from the uncoupled quadricyclane.

1. Introduction

Strong light-matter coupling has gained increasing attention in recent years as it provides new means to modify chemical and physical properties of molecules without changing their structure.^[1] The coupling is achieved by placing the molecules inside an optical cavity, which changes the electromagnetic environment. If the energy of a cavity mode is on resonance with a molecular transition and their coupling is strong enough, two new hybrid states are formed, called polaritons (Figure 1a,b). Their hybrid photonic and molecular character results in unique properties such as a delocalized and dispersive behavior. Their impact on energy transfer,^[2] emission quantum yield,^[3] and excited state lifetime^[4] has been investigated. Furthermore, applications like polariton lasing^[5] and room temperature Bose-Einstein condensation^[6] in the strong coupling regime have been achieved, showing a diverse usefulness of polaritons.

Recently, the effect of strong coupling on chemical reactivity has come more into focus, either coupling to vibrational or electronic states.^[7] The effect of vibrational strong coupling on chemical reactivity has been investigated experimentally^[8] and theoretically.^[9] Strong coupling to electronic transitions alters the excited state potential energy surface, and thus modifies photochemical reactions.^[10] For instance, the suppression of photo-oxidation of an organic dye has been reported.^[11] Also the effect on reverse intersystem crossing^[12] and on triplet-triplet annihilation photon upconversion^[13] has been explored. Furthermore, theoretical aspects of excited state chemistry in the strong coupling regime are well developed.^[10c,14] Photoisomerization reactions act as a testbed for theoretical investigations.^[10a,15] Experimentally, the strong coupling regime has been demonstrated to modify the kinetics of a photoisomerisation reaction.^[10d] However, photoisomerization efficiency as the most important parameter of a photo-switchable molecule has never been in focus.

The norbornadiene–quadricyclane (NBD–QC) photoswitch couple has been applied in molecular logics,^[16] molecular electronics,^[17] and molecular thermal energy storage schemes.^[18] After excitation, NBD converts into its QC isomer by an intramolecular [2 + 2] cycloaddition (Figure 1c). The ring tension in QC

J. Mony, Dr. K. Börjesson
Department of Chemistry and Molecular Biology
University of Gothenburg
Gothenburg 412 96, Sweden
E-mail: karl.borjesson@gu.se

Dr. C. Climent, Dr. J. Feist
Departamento de Física Teórica de la Materia Condensada
and Condensed Matter Physics Center (IFIMAC)
Universidad Autónoma de Madrid
Madrid E-28049, Spain
E-mail: johannes.feist@uam.es

Dr. A. U. Petersen, Prof. K. Moth-Poulsen
Department of Chemistry and Chemical Engineering
Chalmers University of Technology
Gothenburg 412 96, Sweden

 The ORCID identification number(s) for the author(s) of this article can be found under <https://doi.org/10.1002/adfm.202010737>.

© 2021 The Authors. Advanced Functional Materials published by Wiley-VCH GmbH. This is an open access article under the terms of the Creative Commons Attribution-NonCommercial License, which permits use, distribution and reproduction in any medium, provided the original work is properly cited and is not used for commercial purposes.

DOI: 10.1002/adfm.202010737

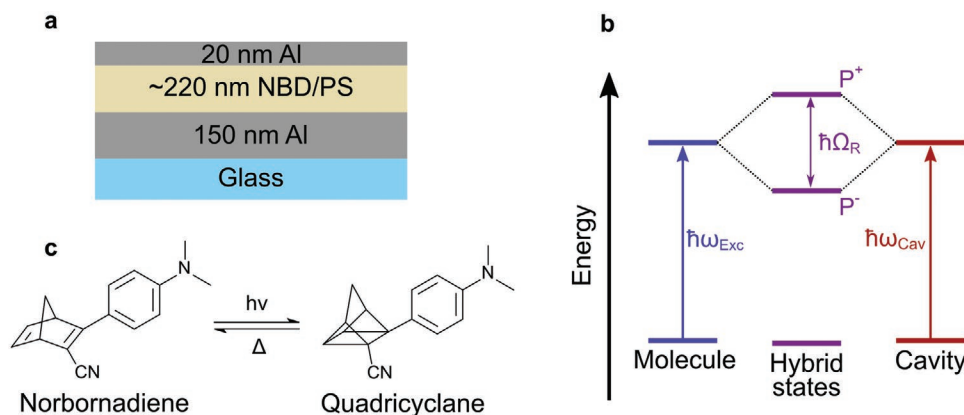


Figure 1. a) The structure of the Fabry–Pérot cavities used in this study. b) Energy diagram showing the hybridization between a molecular transition and a cavity mode leading to the formation of two polaritonic states (P^- and P^+) separated in energy by the Rabi splitting ($\hbar\Omega_R$). c) The photoisomerization process of the norbornadiene derivative to its quadricyclane isomer.

leads to a higher ground state energy compared to NBD, thus, QC is meta-stable and converts back to NBD thermally. A limiting factor in obtaining high-performance systems is to synthesize NBD derivatives that feature a good solar spectrum match and a long-term energy storage at the same time.^[19] Unsubstituted NBD has an absorption onset at 267 nm, but the solar radiation is weak below 300 nm. Therefore, large efforts have been made to synthesize derivatives showing a red shift in their absorption properties.^[18] The most successful method involves introducing electron donating and electron withdrawing substituents, resulting in a push-pull conjugated system.^[18] However, by shifting the absorption further using a strong push-pull system, the thermal stability of the QC state in many cases becomes too low for the couple to be of practical use.^[20] While structural modifications of the system have shown that the thermal stability can be improved,^[19] it is very intriguing to investigate if the thermal stability can be enhanced by other approaches.

A different approach, studied in this work, is to modify the energetics by strong light-matter coupling. The formed polaritons are located at higher and lower energies compared to the molecular transition (Figure 1b), thus a redshift in the absorption occurs without changing the structure of the molecule. Furthermore, we show that the quantum yield of photoisomerization is similar compared to a bare molecule when exciting the upper polariton (UP) or the molecular transition. When exciting the lower polariton (LP), the quantum yield is slightly lower and depends on the detuning between the cavity mode and the molecular transition. Interestingly, the stability of QC is unperturbed by the presence of the cavity. This is despite an effective redshift in the absorbance, showing how strong light-matter coupling can enhance system performance beyond traditional chemistry.

2. Results and Discussion

2.1. Introducing the System

In this study, the impact of strong light-matter interaction on the photoisomerization efficiency of a photoswitchable molecule is investigated. The requirements for a suitable molecule to study

this effect can be split into two aspects: First, the molecule needs to be capable to enter the strong coupling regime. To satisfy this condition, the state being coupled must have a large associated transition dipole moment, and the molecule must be processable into a solid film at high concentrations. In this highly viscous environment, the molecule needs to be able to photoisomerize. Second, both the parent molecule and the photoisomer absorb light, and by choosing a photoswitch couple that absorbs at different wavelengths, one molecule can be coupled selectively. We chose to study the photoswitch couple 2-cyano-3-(4(dimethylamino)phenyl) norbornadiene (NBD)–2-cyano-3-(4(dimethylamino)phenyl) quadricyclane (QC; Figure 1c). The absorption spectrum of a highly concentrated thin film of NBD in a polystyrene matrix is displayed in Figure 2a. The absorption is high, centered at 378 nm, and has a relatively broad Gaussian-like spectral envelope, indicating large inhomogeneous broadening. The NBD–QC couple is a negative photochrome, which means that the excitation energy of the parent molecule is smaller compared to the photoisomer. This is caused by breaking down the conjugated system during the photoisomerization process, resulting in a large difference between the excitation energies of the two molecules. Indeed, according to time-dependent density functional theory calculations, the vertical excitation energy to S_1 for the NBD isomer is 3.48 eV (close to the experimental absorption maximum seen

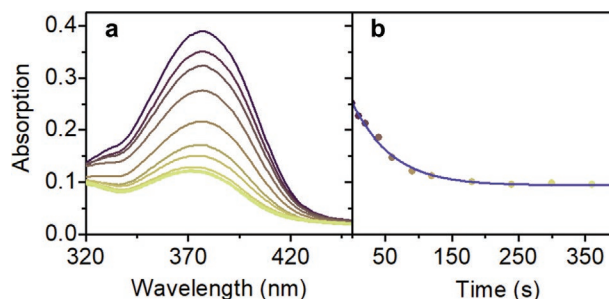


Figure 2. a) Absorption spectra of an NBD film (55% in a polystyrene matrix) after certain times of illumination at 350 nm. b) Measured absorption (dots) at 350 nm over time and a fit using Equation (2) (line) as to determine the photoisomerization quantum yield.

in Figure 2, 378 nm = 3.28 eV), while for the QC isomer it is 4.49 eV. Another important difference between both isomers is that the computed oscillator strength for the $S_1 \leftarrow S_0$ transition of NBD is quite significant, while it is much smaller for QC. When irradiating the NBD film at 350 nm, the absorption decreases due to photoisomerization from NBD to QC. The QC isomer back-converts to NBD thermally. The time scale for the process is given by the half-life of the system, the time at which 50% of the molecules have back-converted. When leaving an irradiated film in the dark, the absorption around 378 nm is slowly regained (Figure S1, Supporting Information), and the estimated half-life is 5.9 ± 0.8 days. The number of converted molecules per absorbed photon defines the photoisomerization quantum yield (Φ) and the change of absorbance over irradiation time can be used to extract the quantum yield from experimental data:^[21]

$$\phi = \frac{\text{\# converted molecules}}{\text{\# absorbed photons}} \quad (1)$$

$$\frac{dAbs}{dt} = -\frac{\phi \cdot \epsilon \cdot 1000 \cdot I \cdot (1 - 10^{-Abs(t)})}{N_A} \quad (2)$$

where t is the time of irradiation, Abs is the absorbance of the film at the wavelength of irradiation, ϵ is the molar absorptivity of the parent molecule ($23\,000 \text{ M}^{-1} \text{ cm}^{-1}$),^[19b] I is the photon flux density ($\approx 1 \cdot 10^{14} \text{ s}^{-1}$), and N_A is the Avogadro constant. The photoisomerization quantum yield of NBD in a polystyrene matrix was determined to be 95%, which is slightly higher than the reported value in toluene solution (78%).^[19b] Exciting the film at different wavelengths results in similar QYs (95% at 380 nm and 96% at 410 nm; Figure S3, Supporting Information). The high photoisomerization efficiency can be explained by the low structural rearrangement in the photoisomerization process as compared to other photoswitch couples. In the NBD/QC couple, two π bonds are converted to two new σ bonds, with no double bond rotation as in *cis-trans* photoswitches, that is, electrons rather than nuclei move during the reaction. Furthermore, both molecules are non-emissive, thus the competitive process lowering the photoisomerization efficiency is vibrational relaxation to the NBD ground state. After long exposure times, a residual absorption around 370 nm is noted in the experiments. Since the absorption is constant with time (after 350 s; Figure 2b), this residual is treated as an offset in the analysis. To conclude, the NBD/QC couple is suitable to study the effect of strong light-matter interactions on the photoisomerization efficiency fulfilling all the described requirements.

2.2. Bare-Molecule Reaction Profile

The calculated energy profile along the isomerization reaction coordinate is shown in Figure 3. It was calculated with the complete active space self-consistent field (CASSCF) method as implemented in the BAGEL program.^[22] The lowest two states were obtained via state-averaged CASSCF. The active space consisted of 14 electrons in 14 orbitals comprising all the π -type orbitals: i) Four from the norbornadiene unit, ii) six from the phenyl ring, and (iii) four from the cyano group. The SVP basis set was used combined with the default density-fitting basis set from the BAGEL library. Geometry optimizations were carried

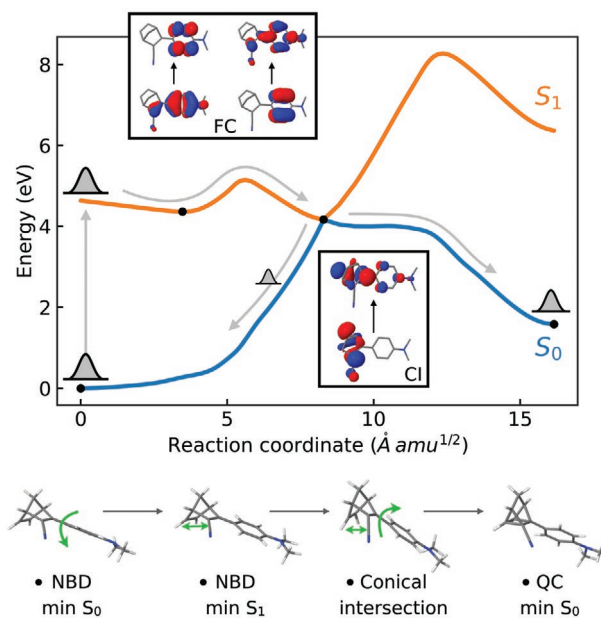


Figure 3. Energy profile for the photoisomerization of 2-cyano-3-(4-(dimethylamino)phenyl) norbornadiene to 2-cyano-3-(4-(dimethylamino)phenyl) quadricyclane calculated with the CASSCF method. Main orbital contributions to the S_1 state at the Franck–Condon (FC) region and at the conical intersection (CI) are also shown as well as the optimized geometries with the principal reaction coordinate shown with green arrows.

out for the ground state of the NBD and QC molecules, as well as the excited singlet state of NBD and the minimum-energy conical intersection. The reaction path was obtained via linear interpolation in internal coordinates between these optimized geometries. Further details on the electronic structure calculations can be found in the Supporting Information. Upon excitation in the Franck–Condon region, the S_1 state of NBD is populated, which mostly involves a π, π^* transition in the phenyl substituent, with a small contribution from the norbornadiene unit. Following the initial excitation, a slight torsion of the phenyl ring relaxes the system to the S_1 minimum. In order to reach the conical intersection where non-radiative relaxation leads to the formation of the QC isomer, an energy barrier must be surmounted. According to our calculations, the barrier from the FC region is 0.57 eV while that from the S_1 minimum configuration is 0.84 eV. Along the path from the S_1 minimum to the conical intersection, the distance between the two double carbon bonds of the NBD unit decreases from ≈ 2.47 to ≈ 2.00 Å. As the barrier is crossed, the S_1 state acquires more π, π^* character on the NBD core. At the optimized conical intersection, the S_0 and S_1 states are degenerate and they mainly correspond to a mixture of the closed-shell configuration with a doubly occupied HOMO and the single-excited HOMO-to-LUMO configuration (Figure 3). At this particular point, relaxation to the ground state potential energy surface is very efficient, where the conversion of the two π bonds to two new σ bond leads to the formation of the QC isomer.

2.3. Entering the Strong Coupling Regime

The large transition dipole moment of NBD enables the strong light-matter coupling regime to be reached. The coupling is

obtained by placing the NBD/polystyrene thin film within a Fabry–Pérot cavity (Figure 1a). The cavity consists of a 20 nm Al top mirror and a 150 nm Al bottom mirror sandwiching the molecular film. The optical cavity confines the electromagnetic field at the optical resonance dictated by the cavity thickness. When the optical resonance matches the molecular transition and the interaction rate is faster than the respective decay rates, the strong coupling regime is achieved. This leads to the formation of two polaritons, whose energetic separation is known as the Rabi splitting ($\hbar\Omega_R$ in Figure 1b). An interesting aspect that must be kept in mind is that the photoisomerization of a molecule is a single-molecule event while the polaritons are delocalized over all molecules coupled to the cavity mode. Thus, for a photoisomerization reaction to occur after excitation of a polariton, a connection between the delocalized polariton and a molecule-centered potential energy surface must be present. This connection is a function of polariton composition. The relative matter and photon contribution of each polariton depends on the energy detuning. When the energies of the molecular transition (E_{Exc}) and the cavity resonance (E_{Cav}) match perfectly, the excitonic and photonic contribution to both polaritons are equal. By changing the cavity thickness, the energy of the cavity mode is varied and thus a mismatch of the two energies is introduced. The bigger the mismatch of the energies, the larger the difference between the two contributions. Figure 4a,c displays the angle-resolved reflectivity of two cavities with slightly different film thicknesses. The molecular transition is clearly replaced by two polariton branches, the UP at high energies and the LP at low energies. The polariton energies increase with angle of incidence due to the cavity mode dispersion. The LP approaches the energy of the molecular transition but never crosses it, and the UP follows the cavity resonance at large angles. The observed avoided crossing is characteristic for a strongly coupled system.

The magnitude of the coupling strength, the Rabi splitting, is defined as the minimal splitting between the two polariton branches and was determined by fitting the polariton branches to a coupled harmonic oscillator model. The Rabi splitting is 591 and 589 meV for the blue detuned ($E_{\text{Cav}} > E_{\text{Exc}}$; Figure 4a) and on-resonance ($E_{\text{Cav}} \approx E_{\text{Exc}}$; Figure 4c) cavities, respectively. A common definition for entrance into the strong coupling regime is to compare the Rabi splitting with the full width half maximum (FWHM) of the molecular transition and cavity resonance. For both cavities, the Rabi splittings are larger than the FWHM of the molecular transition 530 meV and the cavity resonance 390 meV, indicating that the system is under strong coupling. The Hopfield coefficients represent the relative molecule-photon contributions to the polaritons. The molecular contribution to the LP is 62% and 53% for the blue-detuned and on-resonance cavities, respectively. We will later discuss these relative contributions together with the energetics of the LP in relation to the observed photoisomerization efficiency. We already note that large inhomogeneous broadening and the associated significant overlap between the polariton and bare-molecule absorption spectra, as in the present case, has a strong influence on the polariton dynamics, as it can prevent the formation of idealized polaritons and cause rapid decoherence of the polariton into “dark” molecular modes.^[14b,23] The large bandwidth of NBD’s absorption band, which is due to

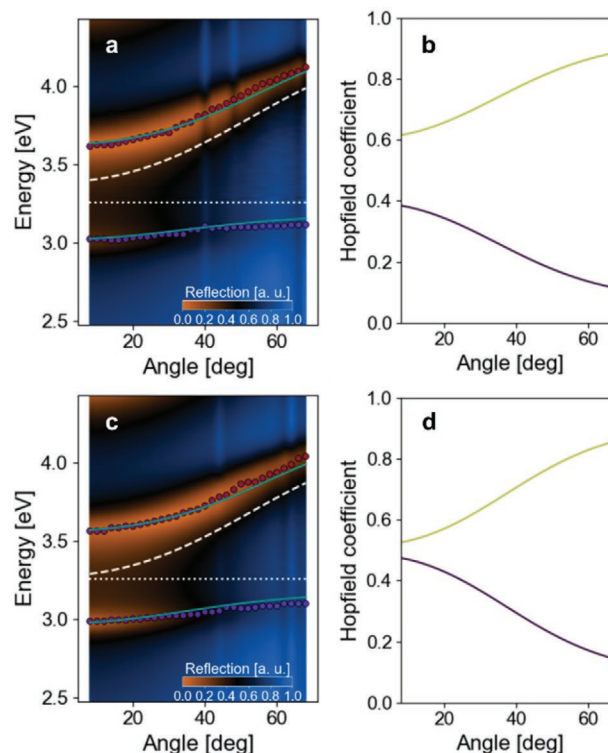


Figure 4. Dispersion plot of a) a blue-detuned and c) an on-resonance sample. The points represent the measured polaritonic peaks and the teal line is a fit using a coupled harmonic oscillator model. The white dashed line shows the energy of the cavity mode and the dotted line the energy of the molecular transition. The excitonic (yellow) and photonic (purple) contribution to the lower polariton is shown for the b) blue detuned and d) on-resonance cavities.

several factors such as vibrational broadening, disorder, and thermal fluctuations, can be represented approximately through a random energy shift (i.e., inhomogeneous broadening) of the molecular transition energies.

2.4. Photoisomerization in the Strong Coupling Regime

Strong light-matter interactions offer a unique way of manipulating excited state energetics without the need of molecular synthesis. Here, we will explore how these hybrid light-matter states connect to a photoisomerization reaction as a molecule-centered event. Figure 5 displays the reflectivity of the two cavities as a function of irradiation time. A decrease in the Rabi splitting is observed for both cases with irradiation time (Figure 5a,c). This reduction is caused by photoisomerization of NBD into QC. The conversion lowers the NBD concentration and therefore the Rabi splitting. From these results, we can already conclude that excitation to polaritonic states allows photoisomerization to occur. For a quantitative measure of the photoisomerization efficiency, Equation (2) cannot be used because the absorbance from the system is not directly translated to a molecular concentration, that is, the Beer–Lambert law is not applicable. Instead, the definition of the photoisomerization quantum yield was used (Equation (1)), and the

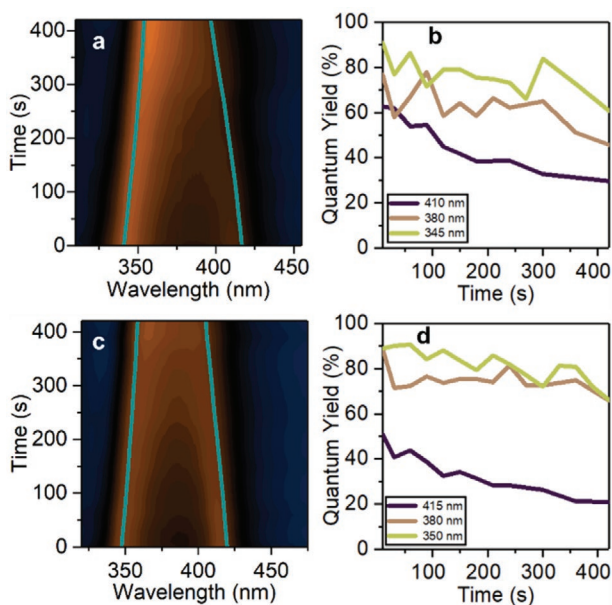


Figure 5. 2D plots of the photoisomerization process of a) the blue-detuned and c) the on-resonance cavities. The teal line shows the peak positions extracted from fitting the measurements with the sum of two Lorentzians. b,d) Diagrams showing the determined quantum yield after each time step, when exciting at the initial wavelength of the upper polariton (yellow), the excitonic peak of the molecule (orange), and the initial wavelength of the lower polariton (purple), for the blue-detuned (b) and on-resonance (d) cavities.

absorbed photons and converted molecules were determined in a short time interval (t). The number of absorbed photons was taken as the photon flux density ($\approx 1 \cdot 10^{14} \text{ s}^{-1}$) times the average absorption over the time interval. Furthermore, the proportional relation between the Rabi splitting ($\hbar\Omega_R$) and the square root of the molecular concentration (c) was used to determine the number of converted molecules:

$$c_t = c_{t=0} \cdot \left(\frac{\hbar\Omega_{R,t}}{\hbar\Omega_{R,t=0}} \right)^2 \quad (3)$$

The Rabi splitting was obtained by fitting the reflectance of the cavities to the sum of two Lorentzians. The teal lines in Figure 5a,c show the peak maxima of the two Lorentzians, and the peak-to-peak energy represents the Rabi splitting. A slight difference in energies between the Lorentzian peak maximum and the reflectivity of the cavities can be noticed (Figure 5; Figure S4, Supporting Information). This is due to the use of two complex Lorentzian resonances with a relative phase between them, which correctly describes the interference between the two resonances. In addition, the quantum yield of photoisomerization lowers with irradiation time in the analysis. This is due to the presence of a residual absorbance after long irradiation times (Figure 2b), which is not taken into account in the analysis and therefore introduces an increasing bias at long irradiation times.

Figure 5b,d displays the quantum yield of isomerization for the two cavities when exciting at the UP energy, at the energy of the molecular transition, and at the LP energy. When exciting

the UP or at the energy of the molecular transition, photoisomerization quantum yields are in the 70–90% range. This is comparable to the photoisomerization quantum yield of a bare NBD film in absence of a cavity (95%). In the analysis, the absorbance of the cavity mirrors is not taken into account (an Al mirror absorbs about 8% of incoming light). The photoisomerization efficiency therefore seems to be unperturbed in the strong coupling regime within the measurement error. On the contrary, when exciting the LP, a reduction of the photoisomerization quantum yield is observed. Furthermore, this reduction is larger in the on-resonance cavity as compared to the blue-detuned cavity. In the on-resonance cavity, the LP has a smaller molecular contribution and is located at lower energy compared to the blue-detuned one. The molecular contribution to the LP affects the system's ability to connect the delocalized polaritonic state to the molecular centered photoisomerization reaction. Furthermore, the lowering of the energy can introduce an additional energetic barrier for the photoisomerization process from the polariton state,^[10a] which will be dependent on the energy of the LP. For the backconversion, the rate-limiting step is to overcome the energy barrier from the ground state of QC back to NBD's ground state (Figure 3). The half-lives for the strongly coupled system (7.8 ± 1.0 days) and the bare film (5.9 ± 0.8 days) are comparable (Figure S1, Supporting Information), thus it can be concluded that the ground state of QC and the energy barrier for thermal backconversion to NBD are unperturbed by strongly coupling the NBD transition.

2.5. Theoretical Discussion

We here discuss the theoretical interpretation of the observed experimental results. The main points to note are that i) the quantum yield when exciting the system at the LP energy is reduced, and ii) the quantum yield when exciting the system at the UP or at the bare-molecule energy is mostly unchanged from the bare system. The first effect is more pronounced when the cavity is on resonance with the molecular absorption peak compared to when it is blue-detuned. The reduction in quantum yield could possibly be due to a collective protection effect in which the LP PES develops a new barrier that the nuclei have to overcome after photoexcitation.^[10a] However, this effect only becomes efficient when the polariton is energetically well-separated from the molecular dark states whose density of states is essentially that of the bare molecules. In the present case, the absorption spectrum of the bare molecule is quite broad while the Rabi splitting is not too large, such that the dark states strongly overlap the polaritons. This is demonstrated in Figure 6a, which shows the polaritonic PES under motion of a single molecule in the ensemble in the presence of disorder. Due to the large overlap between the polariton and dark state energies, there is not a single “polaritonic” eigenstate, but a continuum of eigenstates with cavity photon contributions that are concentrated in two energy regions, as demonstrated in Figure 6b. As a consequence, after external excitation of the cavity, there is rapid energy transfer from the “polariton”, which in this case is really a coherent superposition of many mixed states, to the bare-molecule states, even for the “upward” energy transfer from the LP to the dark states.^[14b] At the same time, the polaritons

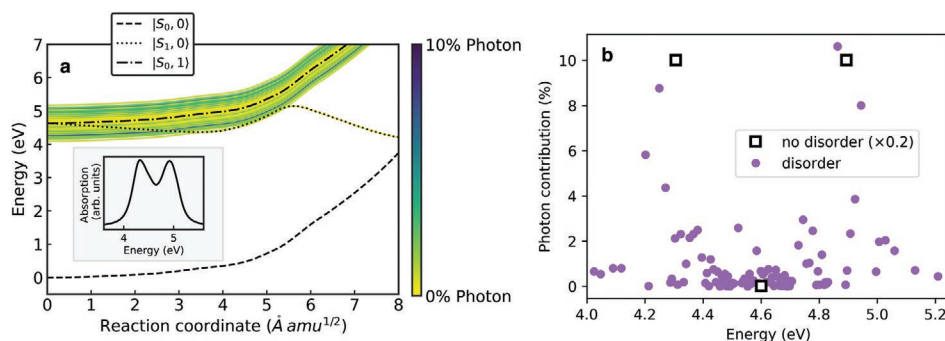


Figure 6. a) Polaritonic potential energy surfaces for motion of a single molecule out of the ensemble (with nuclear motion for all other molecules frozen) in the presence of energetic disorder of the molecules. The inset shows the absorption spectrum, in which a clear Rabi splitting is visible. Panel (b) shows the contributions of the photon mode to the electronic-photonic eigenstates (which determine the polaritonic PES) of the system as a function of the eigenstate energy. We show the result at $R = 0$ under zero detuning, for 100 molecules. Without energetic disorder (squares), only three distinct eigenstate energies appear: The lower and upper polaritons, shifted up and down by half the Rabi splitting from the bare molecule energy, and corresponding to a mixture of 50% cavity and 50% (delocalized) molecular excitation, as well as 99 degenerate dark states at the bare molecule frequency, with 0% cavity photon contribution. In the case with disorder (purple circles), the molecular excitation energies are randomly chosen from a Gaussian distribution. The simple picture of just two distinct types of states does not hold, and the photon mode instead contributes to many system eigenstates to varying degrees. The states with significant photonic part are still concentrated around the energies where lower and upper polaritons would be expected but are not “pure” polaritons.

also decay by rapid photon emission due to the short cavity lifetime. The reduction of the quantum yield when pumping the LP can then be understood as arising from the competition between the decay of the polariton through photon emission and energy transfer to the “dark” or “reservoir” states. Calculating the population dynamics within the model shown in Figure 6, using parameters extracted independently from the experiment without any additional adjustments, predicts a reduction of $\approx 50\%$ for the quantum yield of the LP, consistent with the experimental results (Figure S6, Supporting Information). This picture is also supported by the dependence on cavity tuning, since the photon contribution to the LP is larger for the on-resonance cavity than for the blue-detuned cavity. For the UP, vibration-assisted decay is energetically allowed and thus even more efficient,^[24] such that photon decay becomes less important in comparison. The experimental results imply that energy transfer is sufficiently fast that only a negligible fraction of excitation is lost by photon emission after excitation at the UP energy.

3. Conclusion

In conclusion, the efficiency of a photoisomerization reaction in the strong coupling regime is determined for the first time. For the chosen system, the strong coupling regime does not seem to overly affect the photoisomerization quantum yield when exciting the UP or the energy of the molecular transition. However, when exciting the LP, a reduction in the quantum yield is observed. This reduction is increased when the cavity resonance is shifted to lower energies, highlighting the importance of the photon decay of the cavity mode for excited state reactions in the strong coupling regime.^[11,25] Furthermore, we show that the back reaction is not affected by the strong coupling regime since it occurs on the ground state potential energy surface. The system therefore has a red-shifted onset of absorption and at the same time a retained back reaction. From a molecular solar thermal perspective, these results are highly

interesting. When using “traditional” chemical modifications, it has been shown that the excitation energy and the rate of the thermal backconversion are anti-correlated in the NBD–QC couple, such that improving one causes the other to decline.^[19b] Our results highlight that strong light-matter coupling can circumvent this dilemma, and enable low energy photons to drive a photochemical reaction without perturbing the thermally induced back reaction.

4. Experimental Section

Sample Preparation: Cavities and the bare film were built on glass substrates. The glass plates were cleaned by sonication in an alkaline solution (0.5% of Hellmanex in distilled water) for 15 min, followed by further sonication for 1 h in water and ethanol, respectively. Before use, the cleaned glass substrates were dried in an oven. NBD was dissolved in a solution of polystyrene (22 mg mL⁻¹, Sigma Aldrich) in toluene having a final NBD concentration of 12 mg mL⁻¹. The bare film was deposited from the solution on a glass substrate by spincoating (Laurell Technologies WS-650). For the cavities, the solution was spincoated on an aluminum mirror (150 nm), which was prepared by vacuum sputtering deposition (HEX, Korvus Technologies) on the glass substrates. The thickness of the cavities was varied by changing the rotational speed (2100–2500 rpm) of the spin coating step. Finally, the cavities were sealed by deposition of a second, thinner aluminum mirror (20 nm). If not used immediately after preparation, the samples were stored in the dark under nitrogen.

Sample Characterization: The absorption spectrum of the bare film and the dispersive reflectance spectra of the cavities were measured using a spectrophotometer (LAMBDA 950, PerkinElmer). The reflectance of the cavities was measured through the front thin mirror using a universal reflectance accessory (PerkinElmer). Due to the thicker back mirror, transmission of light was avoided, and the reflectance was directly related to the absorption (reflectance = 1 – absorbance). The concentration (c) of the films was determined by the Beer–Lambert law:

$$c = \frac{Abs(\lambda)}{\epsilon(\lambda) \cdot l} \quad (4)$$

The absorption (Abs) was used from the measurements, the molar absorptivity (ϵ) was taken from literature (23 000 M⁻¹ cm⁻¹)^[19b] and the length (l) was measured with a profilometer (KLA Tencor D-100). The concentration inside the cavities was assumed to be the same.

Photoisomerization Measurements: For the photoisomerization, the light of a xenon lamp inside of a spectrofluorometer (FLS1000, Edinburgh Instruments) was used, which could be set to a desired wavelength. The progress of the photoisomerization was measured by a spectrophotometer (LAMBDA 950, PerkinElmer). For the measurements, the cavities were placed on a reflectivity sample holder with a fixed angle of 6 degree. The cavity on the sample holder was transferred between the spectrofluorometer for exposure and the spectrophotometer to measure the reflectivity, from which the absorption of the system was calculated. The number of absorbed photons was taken as the average absorption in a time interval multiplied by the photon flux density multiplied by the time interval. The energy of the light beam was measured with an optical photometer (Thorlabs), which was used to determine the number of photons and thus the photoisomerization quantum yield.

Coupled Harmonic Oscillator Model: The experimental data were fitted to a coupled harmonic oscillator model.^[26] A 2×2 matrix Hamiltonian describes the coupling between one exciton and one photon:

$$\begin{pmatrix} E_{\text{Cav}}(\theta) & \frac{\hbar\Omega_R}{2} \\ \frac{\hbar\Omega_R}{2} & E_{\text{Exc}} \end{pmatrix} \begin{pmatrix} \alpha \\ \beta \end{pmatrix} = E \begin{pmatrix} \alpha \\ \beta \end{pmatrix} \quad (5)$$

where E_{Exc} is the exciton energy, which was determined experimentally, $\hbar\Omega_R$ is the Rabi splitting, α and β are the mixing coefficients for the system (Hopfield coefficients), and $E_{\text{Cav}}(\theta)$ is the cavity energy, which angle dependence can be calculated by the following equation.

$$E_{\text{Cav}}(\theta) = E_0 \left(1 - \frac{\sin^2 \theta}{n_{\text{eff}}^2} \right)^{\frac{1}{2}} \quad (6)$$

where E_0 is the cavity energy at normal incidence, θ is the incidence, and n_{eff} is the effective refractive index. The obtained fitted parameters for $\hbar\Omega_R$, α , β , and E_0 are summarized in Table S1, Supporting Information.

Strong Coupling Model: To study the strong coupling situation we have relied on the approach based on polaritonic potential energy surfaces.^[7b,10a,c] The Hamiltonian describing N molecules coupled to one cavity mode within the single-excitation subspace and under the rotating wave approximation reads:

$$\hat{H} = \sum_{i=1}^N \hat{H}_{\text{mol}}^{(i)} + \hbar\omega_c \hat{a}^\dagger \hat{a} + \sum_{i=1}^N g^{(i)} (\hat{a}^\dagger + \hat{a}) \quad (7)$$

where \hat{a}^\dagger and \hat{a} are the creation and annihilation operators for the bosonic cavity mode and $\hbar\omega_c$ its energy. The eigenstates of the molecular Hamiltonian in the first term correspond to the S_0 and S_1 energies from electronic structure calculations. The coupling strength $g = \hat{\mu} \cdot \hat{E}_{\text{1ph}}$ is the dot product between the transition dipole moment operator and the single-photon electric field amplitude. The transition dipole moment between the S_0 and S_1 states along the reaction path was calculated and found not to vary much in the region shown in Figure 6. For simplicity, the coupling strength was therefore considered constant and equal for all molecules. In particular, $g = \Omega/2\sqrt{N}$ was taken with the experimental Rabi splitting $\Omega = 0.6$ eV and $N = 100$. The cavity mode was considered resonant with the $S_0 \rightarrow S_1$ vertical transition. To account for inhomogeneous broadening present in the experimental absorption spectrum of the thin film, the S_1 potential energy surface of all the molecules was shifted according to a normal distribution centered at the calculated vertical transition energy and considering the experimental FWHM of 530 meV.

Diagonalizing the strong-coupling Hamiltonian gives $N + 1$ eigenstates. In the absence of disorder, the eigenstates corresponded to two polaritons and $N - 1$ dark states with no cavity component. When considering disorder, the clear distinction between polaritons and dark states is lost, and all states acquire partially photonic character. However, the states with the largest photonic contribution are still concentrated at the energies of the polaritons in the system without disorder. Note

that in Figure 6 the motion of one molecule in the ensemble is plotted, that is, the remaining $N - 1$ molecules were fixed at the ground-state equilibrium position. As a consequence, $N - 1$ copies of the ground state potential energy surface appear shifted by $\hbar\omega_c$ plus the energetic disorder term.^[10a]

Supporting Information

Supporting Information is available from the Wiley Online Library or from the author.

Acknowledgements

K.B. gratefully acknowledges financial support from the European Research Council (ERC2017-StG-757733) and the Knut and Alice Wallenberg Foundation (KAW 2017.0192). J.F. and C.C. acknowledge financial support from the European Research Council through grant ERC-2016-StG-714870, and by the Spanish Ministry for Science, Innovation, and Universities—Agencia Estatal de Investigación through grants RTI2018-099737-B-I00, PCI2018-093145 (through the QuantERA program of the European Commission), and CEX2018-000805-M (through the María de Maeztu program for Units of Excellence in R&D).

Conflict of Interest

The authors declare no conflict of interest.

Data Availability Statement

The data that support the findings of this study are available from the corresponding author upon reasonable request.

Keywords

energy storage, photoisomerization quantum yields, photoswitches, polaritonic chemistry, potential energy surfaces, solar fuels, strong coupling

Received: December 14, 2020

Revised: February 23, 2021

Published online: March 14, 2021

- [1] a) T. W. Ebbesen, *Acc. Chem. Res.* **2016**, *49*, 2403; b) P. Törmä, W. L. Barnes, *Rep. Prog. Phys.* **2014**, *78*, 013901; c) D. G. Lidzey, D. D. C. Bradley, M. S. Skolnick, T. Virgili, S. Walker, D. M. Whittaker, *Nature* **1998**, *395*, 53.
- [2] a) D. M. Coles, N. Somaschi, P. Michetti, C. Clark, P. G. Lagoudakis, P. G. Savvidis, D. G. Lidzey, *Nat. Mater.* **2014**, *13*, 712; b) K. Georgiou, P. Michetti, L. Gai, M. Cavazzini, Z. Shen, D. G. Lidzey, *ACS Photonics* **2018**, *5*, 258; c) X. Zhong, T. Chervy, L. Zhang, A. Thomas, J. George, C. Genet, J. A. Hutchison, T. W. Ebbesen, *Angew. Chem., Int. Ed.* **2017**, *56*, 9034.
- [3] S. Wang, T. Chervy, J. George, J. A. Hutchison, C. Genet, T. W. Ebbesen, *J. Phys. Chem. Lett.* **2014**, *5*, 1433.
- [4] a) D. G. Lidzey, A. M. Fox, M. D. Rahn, M. S. Skolnick, V. M. Agranovich, S. Walker, *Phys. Rev. B* **2002**, *65*, 195312;

- b) J. Mony, M. Hertzog, K. Kushwaha, K. Börjesson, *J. Phys. Chem. C* **2018**, *122*, 24917.
- [5] S. Kéna-Cohen, S. R. Forrest, *Nat. Photonics* **2010**, *4*, 371.
- [6] a) J. D. Plumbhof, T. Stöferle, L. Mai, U. Scherf, R. F. Mahrt, *Nat. Mater.* **2014**, *13*, 247; b) T. Cookson, K. Georgiou, A. Zasedatelev, R. T. Grant, T. Virgili, M. Cavazzini, F. Galeotti, C. Clark, N. G. Berloff, D. G. Lidzey, P. G. Lagoudakis, *Adv. Opt. Mater.* **2017**, *5*, 1700203.
- [7] a) M. Hertzog, M. Wang, J. Mony, K. Börjesson, *Chem. Soc. Rev.* **2019**, *48*, 937; b) J. Feist, J. Galego, F. J. Garcia-Vidal, *ACS Photonics* **2018**, *5*, 205; c) R. F. Ribeiro, L. A. Martínez-Martínez, M. Du, J. Campos-Gonzalez-Angulo, J. Yuen-Zhou, *Chem. Sci.* **2018**, *9*, 6325.
- [8] a) A. Thomas, J. George, A. Shalabney, M. Dryzhakov, S. J. Varma, J. Moran, T. Chervy, X. Zhong, E. Devaux, C. Genet, J. A. Hutchison, T. W. Ebbesen, *Angew. Chem., Int. Ed.* **2016**, *55*, 11462; b) A. Thomas, L. Lethuillier-Karl, K. Nagarajan, R. M. A. Vergauwe, J. George, T. Chervy, A. Shalabney, E. Devaux, C. Genet, J. Moran, T. W. Ebbesen, *Science* **2019**, *363*, 615; c) T. Anoop, J. Anjali, L.-K. Lucas, M. A. V. Robrecht, N. Kalaivanan, D. Eloise, G. Cyriaque, M. Joseph, W. E. Thomas, *Nanophotonics* **2020**, *9*, 249; d) J. Lather, P. Bhatt, A. Thomas, T. W. Ebbesen, J. George, *Angew. Chem., Int. Ed.* **2019**, *58*, 10635; e) K. Hirai, R. Takeda, J. A. Hutchison, H. Uji-i, *Angew. Chem., Int. Ed.* **2020**, *59*, 5332; f) R. M. A. Vergauwe, A. Thomas, K. Nagarajan, A. Shalabney, J. George, T. Chervy, M. Seidel, E. Devaux, V. Torbeev, T. W. Ebbesen, *Angew. Chem., Int. Ed.* **2019**, *58*, 15324.
- [9] a) J. A. Campos-Gonzalez-Angulo, R. F. Ribeiro, J. Yuen-Zhou, *Nat. Commun.* **2019**, *10*, 4685; b) J. Galego, C. Climent, F. J. Garcia-Vidal, J. Feist, *Phys. Rev. X* **2019**, *9*, 021057; c) C. Climent, J. Galego, F. J. Garcia-Vidal, J. Feist, *Angew. Chem., Int. Ed.* **2019**, *58*, 8698; d) T. E. Li, A. Nitzan, J. E. Subotnik, *J. Chem. Phys.* **2020**, *152*, 234107; e) V. P. Zhdanov, *Chem. Phys.* **2020**, *535*, 110767.
- [10] a) J. Galego, F. J. Garcia-Vidal, J. Feist, *Nat. Commun.* **2016**, *7*, 13841; b) J. Galego, F. J. Garcia-Vidal, J. Feist, *Phys. Rev. Lett.* **2017**, *119*, 136001; c) J. Galego, F. J. Garcia-Vidal, J. Feist, *Phys. Rev. X* **2015**, *5*, 041022; d) J. A. Hutchison, T. Schwartz, C. Genet, E. Devaux, T. W. Ebbesen, *Angew. Chem., Int. Ed.* **2012**, *51*, 1592.
- [11] B. Munkhbat, M. Wersäll, D. G. Baranov, T. J. Antosiewicz, T. Shegai, *Sci. Adv.* **2018**, *4*, eaas9552.
- [12] a) K. Stranius, M. Hertzog, K. Börjesson, *Nat. Commun.* **2018**, *9*, 2273; b) E. Eizner, L. A. Martínez-Martínez, J. Yuen-Zhou, S. Kéna-Cohen, *Sci. Adv.* **2019**, *5*, eaax4482; c) Y. Yu, S. Mallick, M. Wang, K. Börjesson, *ChemRxiv* **2020**, <https://doi.org/10.26434/chemrxiv.12932972>.
- [13] a) C. Ye, S. Mallick, M. Kowalewski, K. Börjesson, *ChemRxiv* **2020**, <https://doi.org/10.26434/chemrxiv.12806861>; b) D. Polak, R. Jayaprakash, T. P. Lyons, L. Á. Martínez-Martínez, A. Leventis, K. J. Fallon, H. Coulthard, D. G. Bossanyi, K. Georgiou, I. I. A. J. Petty, J. Anthony, H. Bronstein, J. Yuen-Zhou, A. I. Tartakovskii, J. Clark, A. J. Musser, *Chem. Sci.* **2020**, *11*, 343; c) A. M. Berghuis, A. Halpin, Q. Le-Van, M. Ramezani, S. Wang, S. Murai, J. G. Rivas, *Adv. Funct. Mater.* **2019**, *29*, 1901317.
- [14] a) F. Herrera, F. C. Spano, *Phys. Rev. Lett.* **2016**, *116*, 238301; b) G. Groenhof, C. Climent, J. Feist, D. Morozov, J. J. Toppari, *J. Phys. Chem. Lett.* **2019**, *10*, 5476; c) M. Du, R. F. Ribeiro, J. Yuen-Zhou, *Chem* **2019**, *5*, 1167.
- [15] a) J. Fregoni, G. Granucci, E. Coccia, M. Persico, S. Corni, *Nat. Commun.* **2018**, *9*, 4688; b) J. Fregoni, G. Granucci, M. Persico, S. Corni, *Chem* **2020**, *6*, 250.
- [16] A. Dreos, Z. Wang, B. E. Tebikachew, K. Moth-Poulsen, J. Andréasson, *J. Phys. Chem. Lett.* **2018**, *9*, 6174.
- [17] H. B. Li, B. E. Tebikachew, C. Wiberg, K. Moth-Poulsen, J. Hihath, *Angew. Chem., Int. Ed.* **2020**, *59*, 11641.
- [18] J. Orrego-Hernández, A. Dreos, K. Moth-Poulsen, *Acc. Chem. Res.* **2020**, *53*, 1478.
- [19] a) M. Mansø, A. U. Petersen, Z. Wang, P. Erhart, M. B. Nielsen, K. Moth-Poulsen, *Nat. Commun.* **2018**, *9*, 1945; b) M. Jevric, A. U. Petersen, M. Mansø, S. Kumar Singh, Z. Wang, A. Dreos, C. Sumbly, M. B. Nielsen, K. Börjesson, P. Erhart, K. Moth-Poulsen, *Chem. - Eur. J.* **2018**, *24*, 12767.
- [20] M. Sadao, A. Yoshinobu, Y. Zen-ichi, *Chem. Lett.* **1987**, *16*, 195.
- [21] K. Stranius, K. Börjesson, *Sci. Rep.* **2017**, *7*, 41145.
- [22] a) Brilliantly Advanced General Electronic-structure Library, <http://www.nubakery.org> (accessed: December 2020); b) T. Shiozaki, *Wiley Interdiscip. Rev.: Comput. Mol. Sci.* **2018**, *8*, e1331.
- [23] a) R. Houdré, R. P. Stanley, M. Ilegems, *Phys. Rev. A* **1996**, *53*, 2711; b) P. Michetti, G. C. La Rocca, *Phys. Rev. B* **2005**, *71*, 115320; c) P. Michetti, L. Mazza, G. C. La Rocca, in *Organic Nanophotonics: Fundamentals and Applications*, (Ed: Y. S. Zhao), Springer, Berlin **2015**, p. 39–68.
- [24] M. Litinskaya, P. Reineker, V. M. Agranovich, *J. Lumin.* **2004**, *110*, 364.
- [25] S. Felicetti, J. Fregoni, T. Schnappinger, S. Reiter, R. de Vivie-Riedle, J. Feist, *J. Phys. Chem. Lett.* **2020**, *11*, 8810.
- [26] M. S. Skolnick, T. A. Fisher, D. M. Whittaker, *Semicond. Sci. Technol.* **1998**, *13*, 645.